INTERFACE FOCUS

The effects of femoral metaphyseal morphology on growth plate biomechanics in juvenile chimpanzees and humans

Journal:	*Interface Focus*
Manuscript ID	RSFS-2020-0092.R2
Article Type:	Research
Date Submitted by the Author:	24-May-2021
Complete List of Authors:	Stamos, Peter; University of Chicago Biological Sciences Division, Department of Organismal Biology and Anatomy Berthaume, Michael; London South Bank University
Subject:	Biomechanics < CROSS-DISCIPLINARY SCIENCES
Keywords:	growth plate, metaphysis, hominoid, locomotor biomechanics, finite element model

Author-supplied statements

Relevant information will appear here if provided.

Ethics

Does your article include research that required ethical approval or permits?:
This article does not present research with ethical considerations

Statement (if applicable):
CUST_IF_YES_ETHICS :No data available.

Data

It is a condition of publication that data, code and materials supporting your paper are made publicly available. Does your paper present new data?:
Yes

Statement (if applicable):
The data and R code utilized in this study are available for download at https://github.com/PAStamos/Hominoid-FEA

Conflict of interest

I/We declare we have no competing interests

Statement (if applicable):
CUST_STATE_CONFLICT :No data available.

Authors' contributions

This paper has multiple authors and our individual contributions were as below

Statement (if applicable):
PAS collected the 3D surface scans of the bones utilized in this study. PAS and MAB both created the FE models, analyzed the results, and wrote the manuscript. Both authors gave final approval for publication.

The effects of femoral metaphyseal morphology on growth plate biomechanics in juvenile chimpanzees and humans

Stamos, Peter A[1*], Berthaume, Michael A[2]

[1]Department of Organismal Biology and Anatomy, University of Chicago, Chicago, Illinois, USA

[2]Division of Mechanical Engineering and Design, London South Bank University, London, UK

*corresponding author

Email: pstamos@uchicago.edu

Address:

Anatomy
1027 E 57th Street
Chicago, IL 60637

Keywords
growth plate, metaphysis, hominoid, locomotor biomechanics, finite element model

Abstract

The distal femoral metaphyseal surface presents dramatically different morphologies in juvenile extant hominoids – humans have relatively flat metaphyseal surfaces when compared to the more complex metaphyseal surfaces of apes. It has long been speculated that these different morphologies reflect different biomechanical demands placed on the growth plate during locomotor behavior, with the more complex metaphyseal surfaces of apes acting to protect the growth plate during bent-kneed behaviors like climbing. To test this hypothesis, we built subject-specific parametric finite element models from the surface scans of the femora of 5 *Pan* and 6 *Homo* juveniles. We then simulated the loading conditions of either a straight-legged walking or a bent-kneed climbing gait and measured the resulting stresses at the growth plate. When subjected to the simulated climbing loading conditions, both maximum and mean von Mises stresses were significantly lower in the *Pan* models relative to the *Homo* models. Further, during these loading conditions, von Mises stresses were strongly negatively correlated with ariaDNE, a measure of complexity of the metaphyseal surface. These results indicate that metaphyseal surface morphology has a robust effect on growth plate mechanics.

Introduction

Locomotor biomechanics can have significant effects on skeletal morphology, particularly during growth and development (1–3). In mammalian taxa, many bones – including the femur – grow in length by depositing bone on the metaphyseal surface at the site of the cartilaginous growth plate, pushing the epiphysis further out and increasing the bone's length. Skeletal maturity is reached when the epiphysis fuses to the metaphysis, ceasing longitudinal growth and "erasing" the cartilaginous growth plate.

As juvenile bone, and the growth plate in particular, is relatively compliant (4), it is likely juvenile bone and the growth plate (and thereby, the metaphyseal and epiphyseal surfaces) may have been targeted by natural selection to be especially influenced by locomotor biomechanics (1).

Metaphyseal surface morphology and locomotion

The morphology of the distal femoral metaphyseal surface is highly variable across juvenile mammals. Thomson (5) provided the first description of these differences, noting how some mammals possessed relatively flat surfaces, while others possessed topographically complex surfaces with bony projections and recesses. In all cases, the surface of the epiphysis mirrored the surface of the metaphysis (Figure: 1). Thomson argued that the same physical laws govern the functional requirements of juvenile and adult bones, and thus morphological variation in metaphyseal and epiphyseal surfaces likely served a biomechanical function. He proposed differences in morphology reflected differences in knee joint loads engendered by locomotory kinematics. Specifically, he speculated that animals that engaged in more bent-knee gaits, like sheep and wolves, experience more shear forces at the growth plate during locomotion, and thus require a more complex metaphyseal surface with significant metaphyseal and epiphyseal surface interdigitation to resist antero-posteriorly oriented forces and prevent the epiphysis from slipping off. Conversely, animals that engaged in more straight-legged gaits, such as humans and

elephants, experience more compressive forces at the growth plate during locomotion, and there is little need for bony structures to resist antero-posteriorly oriented shear forces.

Subsequent to Thomson's 1902 work, there was very little discussion of metaphyseal surface morphology in comparative anatomy until recently. Tardieu and Preuschoft (6) discovered that extant hominoid distal femoral metaphyseal surfaces can vary dramatically, with juvenile humans having relatively flat surfaces but juvenile apes having relatively complex surfaces (6,7) (Figure: 2). Similar to Thomson, Preuschoft and Tardieu (7) reasoned that the more complex metaphyseal surfaces of apes acted to protect their growth plates during bent-kneed behaviors such as climbing. As Thomson did before them, Preuschoft and Tardieu believed that bent-kneed behaviors would result in large shearing forces acting across the growth plate and thought that the different "facets" present on the distal femoral metaphyseal surface of the femur were situated to be roughly normal to joint reaction forces in different postures.

Stamos and Weaver (8) provided the first systematic survey of metaphyseal surface ontogeny in hominoids. They examined how the distal femoral metaphyseal surface developed from the fetal period until growth plate fusion in *Pongo*, *Gorilla*, *Pan*, and *Homo*. They found (1) all hominoids are born with relatively flat distal femoral metaphyseal surfaces, (2) metaphyseal morphology is correlated with locomotor mode in hominoids, and (3) intraspecific changes in morphology cooccurred with ontogenetic locomotor changes. For instance, all hominoids are born with relatively flat distal femoral metaphyseal surfaces, and only after the onset of independent locomotion do surface morphologies diverge. Further, as locomotor behavior continues to change through ontogeny, metaphyseal surface morphology appears to reflect these changes. This is well demonstrated by *Gorilla*, which are primarily arboreal in the first two years of life, after which they rather abruptly transition to nearly entirely terrestrial knuckle-walking (9). Concurrent with this, Stamos and Weaver documented a clear shift from a more *Pongo*-like "arboreal" morphology in young *Gorilla* individuals to a morphology unique to older, knuckle-walking *Gorilla* individuals. The close relationship between form and function in the metaphyseal surface is likely due to the developmental plasticity of the trait (8).

Biomechanics of the growth plate

As the metaphyseal and epiphyseal surfaces are formed by the growth plate, the relationship between form and function only holds true if the growth plate differentially responds to biomechanical loads. Several studies have discussed the relationship between metaphyseal morphology and growth plate biomechanics. Firth and Hodge (10) noted how growth plate injuries in the long bones of foals are more common at the proximal compared to the distal ends. They further noted proximal ends tended to be flatter while the distal ends were more complex and suggested that this increased incidence in proximal end injuries may be due to greater chance of shear injury in flatter growth plates. While looking at juvenile humans, Tayton (11) argued that the epiphyseal tubercle and its corresponding metaphyseal hollow act to lock the proximal femoral epiphysis in place, preventing shearing injury of the growth plate. Similarly, Liu et al. (12) reasoned that the reduction in relative height of epiphyseal tubercle with age in humans may cause the higher incidences of slipped capital femoral epiphysis/slipped upper femoral epiphysis (SCFE/SUFE) during adolescence.

Limited experimental work has been conducted investigating the relationship between metaphyseal morphology and growth plate biomechanics. Williams et al. (13) performed *ex vivo* experiments on bovine tibia to investigate how growth plate mechanics were influenced by form. They found a strong relationship between growth plate inclination relative to loads and growth

plate failure, and when loaded in uniaxial compression, bovine growth plates were more likely to fail in areas of high inclination relative to the load vector. They concluded that this was likely due to increased shear stress on the growth plate.

Several model-based approaches have investigated the relationship between growth plate orientation or morphology and stresses. Smith (14,15) produced some of the earliest attempts at this when he used the photoelastic method to demonstrate that growth plates tend to lie perpendicular to principal stresses when bones are loaded, and argued that this orientation acts to minimize shear stresses in the growth plate. More recent computational studies utilizing the finite element (FE) method have confirmed the results of Smith's earlier work. Fishkin et al (16) utilized the FE method to show how metaphyseal surface orientation relative to joint loads predicts growth plate failure in SCFE. Of relevance are two computational papers which included variation in metaphyseal surface and growth plate topography. Gao et al. (17) developed FE models to measure the effects of metaphyseal surface topography on stress distribution across the bovine proximal tibial growth plate under uniaxial compression. They modeled flat, "n", and "m" shaped growth plates and found that hydrostatic and octahedral shear stress distributions did not vary much with growth plate shape, but concluded that this lack of variation was likely due to modeling a small portion of the growth plate. Piszczatowski (18) utilized simplified 2-dimensional geometrical FE models to explore the osteogenic mechanotransducive interplay between biomechanical loadings and growth plate geometry. He found that different load orientations and growth plate morphologies resulted in vastly different distributions of stress within the growth plate.

In sum, previous studies indicate that variation in distal femoral metaphyseal surface morphology has profound consequences in growth plate mechanics, and in particular, stresses. However, no previous study has modeled the effects of metaphyseal morphology on growth plate mechanics in a physiologically or ecologically relevant context.

This study

Here, we investigate the effects of metaphyseal morphology on growth plate stresses in two hominoid genera with divergent locomotor behavioral repertoires using FE analysis (FEA). FEA allows the calculation of stresses and strains for geometrically complex structures, such as the metaphyseal surface, under complex loading conditions, such as those experienced during locomotion (19).

We utilize parametric FE modeling to test the effect of a wide range of morphologies in a controlled manner. Parametric FE models provide the user with the ability to (1) investigate the effect of a wide range of morphologies on biomechanical performance, and (2) allow a single parameter to vary while all other variables are either held constant or allowed to co-vary with that parameter. These models are ideal for querying morphospaces to test biological and evolutionary hypotheses concerning the relationship between form and function. For example, they have been used to investigate the biomechanics of cusp sharpness (20) and cranial robusticity (21) in hominoids, enamel fracture in humans (22), skull shape in bats (23), and shell shape and strength (24) and locomotion in turtles (25).

Here, we construct a parametric model of the distal femur of a juvenile hominoid to test the relationship between metaphyseal surface morphology and growth plate stresses during locomotion in humans (*Homo*) and chimpanzees and bonobos (*Pan*). These taxa are an ideal clade to explore this relationship because despite their close phylogenetic relatedness they engage in highly divergent locomotor behaviors.

Juvenile *Homo* are obligate bipeds, and maximum knee loads during upright, bipedal walking are experienced at or near full extension, with a relatively low range of motion during the stance phase (26). Conversely, juvenile *Pan* engages primarily in arboreal locomotion, with climbing comprising 50-70% of their locomotor repertoire in the first two years of life (9,27). This climbing is characterized by deep knee flexion with a large range of motion (28,29). We hypothesize that during loading conditions simulating bent-knee climbing, growth plate stresses will be lower in the *Pan* models with their more topographically complex metaphyseal surfaces relative to the *Homo* models with their relatively flatter metaphyseal surfaces.

Materials and Methods

Sample

Our sample is composed of 11 individuals (Table: 1). Of the five *Pan* individuals, there are two *Pan troglodytes verus,* one *Pan troglodytes schweinfurthii,* and two *Pan paniscus*. All *Pan* specimens were wild collected. Of the six human individuals, two were from a 20th century industrialized Portuguese population and four were from a North American prehistoric hunter-gatherer population. All the individuals in the sample had all their deciduous dentition in full occlusion, with no eruption of the permanent first molars. This corresponds to Shea's (30) Dental Stage 2, and represents approximately one to three years of age for *Pan,* and two to six years of age for humans (31). All specimens in the sample had well-preserved metaphyseal surfaces and were free from obvious pathology or systemic diseases affecting the skeleton. Each specimen was scanned using a NextEngine HD portable 3D laser surface scanner. Individual scans were initially aligned in ScanStudio HD Pro, then exported as point clouds to Geomagic for outlier point removal, further alignment, and wrapping into a 3D mesh.

Parametric finite element model

We created a parametric FE model of the distal end of a juvenile hominoid femur in ANSYS APDL 19.1 (Figure: 3). In total, 31 parameters were used to describe the complex shape of the metaphyseal surface. To construct a morphologically informed parametric model, values for 27 of these parameters were taken from orthographic projections of the 3D surface models to make specimen-specific FE models of the distal femur for each individual in our sample. Two additional parameters were defined relative to a subset of the 27 measurements. The final parameters were defined using measurements of femoral shaft length (50% shaft length) and the mediolateral diameter at 50% shaft length. As hominoid epiphyses are not fully ossified at this developmental stage, 50% length was estimated from the metaphyseal surface. Because cartilaginous growth plates are not preserved during skeletal preparation, and hominoid epiphyses are not fully ossified at this developmental stage, we did not have 3D surface scans from which we could model specimen-specific growth plates or epiphyses. Instead, we modeled a 0.3mm thick growth plate to be congruent to the metaphyseal surface. Growth plate thickness was derived from Sissons and Kember (32), who measured the growth plate of a 5 year old human to be 0.5mm thick. As this measurement included the zone of calcified cartilage, which makes up approximately 40% of the thickness of the growth plate and likely has material properties closer to that of bone than cartilage, we chose to model the cartilaginous portion of the growth plate as 0.3mm thick. We also created generalized *Pan* and *Homo* epiphyses from the fully ossified epiphyses of older individual from our sample, and isometrically scaled this epiphysis by the maximum width of the epiphyseal surface. The proximal end of the epiphysis was modified for each specimen to mirror the distal metaphyseal surface and growth plate of that

specimen. This ensured that the growth plate was sandwiched fully between the distal metaphyseal surface and proximal end of the distal epiphysis, as is the case in living juveniles. Models were meshed with solid185 4-noded, tetrahedral elements. A mesh size of ½ growth plate thickness ($0.15\ mm$) was used for the growth plate, and 2* growth plate thickness ($0.6\ mm$) was used for the rest of the model (model size: ~750,000-1,000,000 elements). No convergence test was run, as it would be impractical to increase mesh size due to computational limitations.

All materials were modeled as linearly elastic with isotropic, homogeneous material properties (18,33). While juvenile bones and growth plates exhibit viscoelastic properties due to increased collagen content, and thus are not linearly elastic, the assumption made in material property model here is appropriate for comparative purposes. The growth plate is nearly incompressible and was assigned mechanical properties following Piszczatowski (18,33) ($E = 6\ MPa, \nu = 0.495$). The epiphysis and distal end of the femoral shaft are primarily trabecular bone with a thin cortical shell, and as such were assigned mechanical properties in line with that of trabecular bone ($E = 345\ MPa, \nu = 0.3$). The only portion of the model that was cortical bone was the femoral shaft. Given the lack of data on juvenile *Pan* and *Homo* cortical bone mechanical properties in the femur, and not wishing for artificial stress concentration to occur due to C^0 continuity in mechanical properties between the femoral shaft and distal end of the femoral shaft, we assigned the femoral shaft the same mechanical properties as trabecular bone ($E = 345\ MPa, \nu = 0.3$).

Each specimen's model was assigned two sets of boundary conditions mimicking a straight-legged "walking" gait, and a 90-degree flexed-knee "climbing" gait. Tibiofemoral and patellofemoral joint reaction forces (JRF) were derived from human locomotor trials in Trepczynski et al. (34) and represent the period of peak JRFs in each gait cycle. The "walking" and "climbing" boundary conditions are obtained from the "walk" and "stair climb" trials, respectively. Constraints were applied to the proximal end of the femur, preventing translation and rotation in all directions and about all axes. A set of exterior nodes representing patellar and tibial contacts were selected, JRFs were distributed evenly over these nodes. For walking, the patellar contacts were approximated to be the top margin of the patellar trochlea (35), and the tibial contacts were approximated to be the distal end of the epiphysis. For climbing, the patellar contacts were approximated to be the anterior to intercondylar notch (35), and the tibial contacts were approximated to be the posterior surface of the femoral condyles. Patellar loads were applied roughly perpendicular to the surface of the model (36), while tibial loads were applied perpendicular to the femoral shaft during climbing, and parallel to the femoral shaft during walking. The magnitude of these forces was based on percent body mass (body weight, BW) following Trepczynski et al. (34). For walking, maximum forces occur at 8° flexion ($tibial\ force\ (TF) = 3.2 * BW, patellar\ force\ (PF) = 0.4 * BW$). For climbing, maximum forces occur at 90° flexion ($TF = 3.7 * BW, PF = 2.7 * BW$). Body mass was estimated to be 20 kg, based on the average weight (50th percentile) of a 5 year-old child in the United Kingdom.

The primary metric we used to evaluate model performance was maximum von Mises stress in the growth plate. Von Mises stress (or octahedral shear stress) is a scalar measure of the magnitude of the distortional component of the multiaxial stress tensor. Because cartilage is nearly incompressible due to its high proteoglycan and water content, hydrostatic compressive stress is well tolerated. On the other hand, distortional stress must be resisted by tensile forces in the collagen component of cartilage, and thus in a complex multiaxial load state cartilage failure is well-approximated by the von Mises stress metric (1). Biological materials like cartilage do

not always fail due to peak stresses – cyclical loading of these materials at submaximal loads can lead to accumulated fatigue and eventual failure. Therefore, we also looked at the effect of metaphyseal morphology on mean von Mises stress (1). To exclude singularities due to boundary conditions, free surfaces, or sharp angles in geometry, we disregarded the 2% elements by volume with the highest stresses and report on 98% von Mises stresses.

To ensure comparability of performance metrics across specimens, stresses were scaled following the formula

$$\sigma = \frac{SA_A}{SA_B}\sigma_A$$

Where σ is the scaled stress, SA_A and σ_A are the surface area and max or mean stress of the model being scaled, and SA_B is the surface area of the model all subsequent models are being scaled to (37). Instead of scaling to the entire surface area of the model, we scaled relative to the surface area of the metaphyseal surface of the growth plate. This ranged from $250.31 - 967.74\ mm$. We chose our reference model (model B) to be the largest individual in our dataset ($967.74\ mm$).

We quantified metaphyseal surface topography of the original 3D surface scan models in our sample using a robustly implemented algorithm for Dirichlet energy of the normal (ariaDNE) (38). Based on Dirichlet Normal Energy (DNE) (39), ariaDNE provides a metric of topographic complexity by measuring how much a surface mesh deviates from a plane. Curvier surfaces have higher normal energy values. Unlike the original DNE metric, ariaDNE can be tuned to be sensitive to only surface details of the scale of interest to the researchers by changing the ε (bandwidth) parameter on a Gaussian kernel function. The current study used ε = 0.10, as that value was previously determined to best capture the larger-scale metaphyseal surface features of interest in this study (8). For a more thorough discussion of the ariaDNE metric and its application to metaphyseal surface morphology, see Stamos and Weaver (8).

We statistically modeled how maximum and mean von Mises stress at the growth plate varied with taxon and loading condition with a generalized linear model implemented in R software v. 3.5.2 (40) with the "Rethinking" package (41). We similarly modeled the relationship between ariaDNE values and maximum and mean von Mises stresses in the walking and climbing models.

Results

The maximum von Mises stress experienced at the growth plated varied significantly with taxon and loading condition (Tables: 1, 2, and 3 and Figures: 4 and 5). Maximum von Mises stresses at the growth plate were similar between the *Homo*-walk models (mean = 0.063 MPa; 95% CI = 0.051, 0.075) and the *Pan*-walk models (mean = 0.074 MPa; 95% CI = 0.061, 0.087). In contrast, the *Pan*-climb models had notably higher maximum von Mises stresses (mean = 0.119 MPa; 95% CI = 0.106, 0.132) than both genera's walking models, while the *Homo*-climb models had the highest maximum von Mises stress (mean = 0.178 MPa; 95% CI = 0.166, 0.190) of any of the four genus and locomotor mode combinations.

Performance for mean von Mises stress was patterned similarly as maximum von Mises stress. The *Pan*-walk (mean = 0.026 MPa; 95% CI = 0.020, 0.032) and *Homo*-walk (mean = 0.030 MPa; 95% CI = 0.024, 0.035) models had similar mean von Mises stresses across the growth plate. The *Pan*-climb models had higher mean von Mises stresses (mean = 0.066 MPa;

95% CI = 0.059, 0.072) than the walking models, and the *Homo*-climb models had the highest mean von Mises stresses (mean = 0.114 MPa; 95% CI = 0.109, 0.120).

The relative performance of each taxon-locomotor mode model can be better appreciated by looking at the ratio of stresses at the growth plate between different sets of models (Tables: 2 and 3). Most notably, maximum von Mises stresses were approximately 50% higher (mean = 1.496; 95% CI = 1.318, 1.698) in the *Homo*-climb models relative to the *Pan*-climb models. The difference was even more stark for mean von Mises stresses, which were about 75% higher (mean = 1.745, 95% CI = 1.570, 1.945) in the *Homo*-climb models relative to the *Pan*-climb models.

Metaphyseal surface topographic complexity, as quantified by the ariaDNE metric, was strongly and consistently negatively correlated with both max and mean von Mises stress in the climbing models (Figure: 6). The relationships between ariaDNE and von Mises stresses during walking are much more equivocal – the maximum *a posteriori* estimate for the mean effect of ariaDNE on mean von Mises stress during walking is negative, however the 95% credibility interval of that effect does include some positive coefficient values. Our analyses show that there is no consistent relationship between ariaDNE and maximum von Mises stress during walking, with the 95% credibility interval for the estimates of the coefficient describing the effect firmly encompassing both negative and positive values.

Discussion

The results of our study clearly indicate that growth plate mechanics are strongly influenced by metaphyseal surface morphology and locomotor mode. Both maximum and mean von Mises stress were consistently much higher during simulated climbing loads relative to walking loads, regardless of metaphyseal surface morphology. However, the more topographically complex *Pan* models experienced considerably lower maximum von Mises stress during climbing than the *Homo* models. There was also a trend towards the *Homo* models having lower maximum von Mises stress during walking relative to the *Pan* models, indicating that perhaps the *Homo* metaphyseal surface is better suited to withstanding loads of a straight-legged gait. However, the magnitude of this effect was not great, and did not reach the traditional levels of statistical significance of $p < 0.05$.

The relationship between both maximum and mean von Mises stress and ariaDNE during climbing but not walking suggests the differences in biomechanical performance between the *Pan* and *Homo* models is driven by differences in metaphyseal complexity. This relationship supports Thompson 1902's hypothesis, showing that metaphyseal shape is related to biomechanical performance, and metaphyses with relatively flat surfaces were less efficient at resisting shear stresses during locomotion than those with relatively complex surfaces. Data from Stamos and Weaver (8) suggests hominoids begin life with a relatively flat metaphyseal surface, which only becomes more complex if adequate shear loads are applied to it. This data shows that having a more complex surface reduces these loads. Together, results from these studies suggest mammals with complex metaphyseal surfaces have undergone large levels of shear loading during their lifetime, and mammals with flat metaphyseal surfaces have not.

Although we focused on *Homo* and *Pan* in this study, these results have implications beyond these taxa, and even primates, and can be generally applied to any animal which utilized growth plates and epiphyses to grow long bones. When combined with information on locomotory kinematics, these data suggest metaphyseal morphology can be a powerful tool for examining locomotory patterns in extinct animals and could be a vital tool for reconstructing

locomotory shifts in fossil taxa, such as the shift from climbing to bipedalism in hominins or in the shift from terrestrial to aquatic locomotion in aquatic and semi-aquatic mammals.

While results are promising, there are several limitations to the current study. We modeled the hominoid distal femur with a simplified, geometrical representation lacking internal geometry and the tissue mechanical properties and model loading conditions were simplified and constant between individuals and taxa. Further, the models were not validated with data derived from *in vivo* or *in vitro* experiments. However, we believe all these above assumptions are appropriate for our study because we are interested in the effect of shape variation on growth plate mechanics. By simplifying the model in this manner, we were able to hold all variables other than the shape of the metaphyseal surface constant. This level of control would not have been possible had we used nonparametric models of real biological specimens with varying material properties.

Our boundary conditions were based on adult, and not juvenile, gait kinematics. Juvenile gaits are highly variable, particularly in mediolateral forces (42,43). The absence of these forces from our model would certainly affect the magnitude of the stresses in our growth plate but are unlikely to significantly affect the results of our comparative analysis. The differences observed between *Pan* and *Homo* were small when anteroposterior shear forces were small (i.e., walking) but large when anteroposterior shear forces were large (i.e., climbing). The addition of another, mediolateral shear force would likely cause even larger differences between our two groups.

Our study is also limited by the fact that our boundary conditions were derived from human subjects performing walking and stair climbing gaits. These forces do not necessarily accurately model hominoid climbing forces in all conditions. However, we believe that they are a reasonable representation of how hominoid knees are loaded during straight-legged and bent-kneed locomotor behaviours in some conditions. The data we used provide a degree of biological realism in lieu of randomly selected forces. Had taxon-specific loading conditions been available to us, we would not have utilized them in this study, as varying the loading conditions between taxa would interfere with our ability to pinpoint differences in stresses due to metaphyseal morphology.

We also only modeled a single point in the locomotor cycle of each behavior. We chose the point that we did because it had the highest reaction forces at the knee, and likely engendered the greatest stresses. Previous work on endochondral mechanotransduction implies that peak stresses have the greatest influence on the bone and chondral modeling response (44), and success has been realized by previous FE studies which utilized the single point in the locomotor cycle with the highest joint reaction forces (45). Our confidence in the models is further bolstered by the fact that the magnitude of stresses we observed are physiologically reasonable and on the order of those which engender differential growth in *in vivo* experiments on immature animal growth plates (46).

Future work should focus on modeling the mechanical performance of the distal femoral metaphyseal surface in other hominoid taxa and age stages. For instance, *Gorilla* are much more arboreal earlier in their juvenile periods relative to later when they engage in more terrestrial knuckle-walking (9). Based on the current study, we would expect that younger *Gorilla* would show better mechanical performance under loads simulating a climbing gait relative to older *Gorilla,* while older *Gorilla* would exhibit better mechanical performance in a knuckle-walking gait relative to younger *Gorilla*. A similar, though less dramatic transition from arboreality to terrestriality is present in *Pan*, and consequently it would be of interest to investigate if the metaphyseal surfaces of older *Pan* individuals are better suited to knuckle-walking than those of

the younger *Pan* modeled in this present study. We are also interested in how the *Homo* metaphyseal surface changes during development. For instance, are younger humans better suited to the "waddling and toddling" (43) gait that characterizes their locomotion relative to adolescents? We also hope to see if we can detect any differences between humans with different subsistence economies and mobility patterns. This study clearly demonstrates the relative performance benefit of more topographically complex metaphyseal surfaces during bent-knee loading conditions. However, we did not detect a clear benefit of the relatively flatter metaphyseal surfaces during straight-knee loading conditions. Future work should focus on determining whether such a performance benefit becomes apparent during higher impact straight-legged loading conditions, such as during bipedal running. Also, if *in vivo* knee forces for different hominoid behaviors become available, we would be interested in seeing how the hominoid growth plate performs under a wide range of positional and locomotor behaviors.

Ultimately, we aim to apply our model to hominoids in the fossil record, such as the DIK-1-1 juvenile *Australopithecus afarensis* individual (47). There is a longstanding and ongoing debate over the locomotor capabilities and habits of the individuals of this species (48–53). We believe that our model of growth plate mechanics can be helpful in determining what sort of loads the DIK-1-1 distal femoral metaphyseal surface developed to withstand, and thus give insight into the locomotor behavioral repertoire of *A. afarensis*.

Conclusions

By utilizing the analytical tools provided by the field of mechanical engineering, we were able to confirm a longstanding hypothesis in mammalogy and anthropology as to the effect of the divergent morphology of the distal metaphyseal surface of the femur on growth plate mechanics in biologically relevant models. Our FE models clearly show that the topographically complex distal femoral metaphyseal surface of juvenile *Pan* individuals acts to reduce stress at the growth plate when engaged in highly flexed-knee locomotor behaviors, such as climbing.

These results further support Stamos and Weaver's (8) argument for the utility of metaphyseal surface morphology in reconstructing locomotor behavior of extinct fossil taxa. By modeling what sort of loads a metaphyseal surface is best fit to resist, one can retrodict what the locomotor repertoire of an extinct individual may have been.

Acknowledgements

We thank each of the following institutes (and their curators and collection managers) for allowing us to study the materials in their care: University of Kentucky (George Crothers), Musée Royal de l'Afrique Centrale (Emmanuel Gilissen and Wim Wendelen), Max Planck Institute (Uta Schwarz), University of Dundee (Craig Cunningham). We also thank three anonymous reviewers for their comments on this study.

Funding

This research has been made possible by funding from the Wenner-Gren Foundation (Grant No. 8868) and the University of California, Davis, Department of Anthropology.

References

1. Carter DR, Beaupré GS. Skeletal Function and Form : Mechanobiology of Skeletal Development, Aging, and Regeneration. New York, NY: Cambridge University Press; 2001.
2. Hamrick MW. A chondral modeling theory revisited. J Theor Biol [Internet]. 1999 Dec 7;201(3):201–8. Available from: http://www.ncbi.nlm.nih.gov/pubmed/10600363
3. Frost HM. From Wolff's Law to the Utah Paradigm: Insights About Bone Physiology and Its Clinical Applications. Anat Rec. 2001;419(February):398–419.
4. Currey JD, Butler G. The mechanical properties of bone tissue in children. J Bone Jt Surg. 1975;57(6):810–4.
5. Thomson A. The Relation of Structure and Function as illustrated by the Form of the Lower Epiphysial Suture of the Femur. J Anat Physiol [Internet]. 1902 [cited 2013 Jan 4];XXXVI:96–105. Available from: http://www.ncbi.nlm.nih.gov/pmc/articles/PMC1287165/
6. Tardieu C, Preuschoft H. Ontogeny of the knee joint in humans, great apes and fossil hominids: pelvi-femoral relationships during postnatal growth in humans. Folia Primatol [Internet]. 1996 Jan [cited 2013 Jan 6];66(1–4):68–81. Available from: http://www.ncbi.nlm.nih.gov/pubmed/8953751
7. Preuschoft H, Tardieu C. Biomechanical reasons for the divergent morphology of the knee joint and the distal epiphyseal suture in hominoids. Folia Primatol [Internet]. 1996 [cited 2014 Jun 13]; Available from: http://medcontent.metapress.com/index/A65RM03P4874243N.pdf
8. Stamos PA, Weaver TD. Ontogeny of the distal femoral metaphyseal surface and its relationship to locomotor behavior in hominoids. Am Assoc Phys Anthropol. 2020;(March):1–13.
9. Doran D. Ontogeny of locomotion in mountain gorillas and chimpanzees. J Hum Evol [Internet]. 1997;32(4):323–44. Available from: http://www.ncbi.nlm.nih.gov/pubmed/9085185
10. Firth EC, Hodge H. Physeal form of the longbones of the foal. Res Vet Sci [Internet]. 1997;62(3):217–21. Available from: http://www.ncbi.nlm.nih.gov/pubmed/9300537
11. Tayton K. Does the upper femoral epiphysis slip or rotate ? J Bone Jt Surg. 2007;1402–6.
12. Liu R, Armstrong D. An Anatomic Study of the Distal Femoral Epiphysis. J Pediatr … [Internet]. 2013;33(7):743–9. Available from: http://europepmc.org/abstract/MED/23812155
13. Williams JL, Vani JN, Eick JD, Petersen EC, Schmidt TL. Shear strength of the physis varies with anatomic location and is a function of modulus, inclination, and thickness. J Orthop Res [Internet]. 1999 Mar;17(2):214–22. Available from: http://www.ncbi.nlm.nih.gov/pubmed/10221838
14. Smith JW. The relationship of epiphysial plates to stress in some bones of the lower limb. J Anat [Internet]. 1962 [cited 2013 Feb 4];96:58–78. Available from: http://www.ncbi.nlm.nih.gov/pmc/articles/PMC1244173/
15. Smith JW. The structure and stress relations of fibrous epiphysial plates. J Anat [Internet]. 1962 Apr;96:209–25. Available from: http://www.pubmedcentral.nih.gov/articlerender.fcgi?artid=1244143&tool=pmcentrez&rendertype=abstract

16. Fishkin Z, Armstrong DG, Shah H, Patra A, Mihalko WM. Proximal femoral physis shear in slipped capital femoral epiphysis--a finite element study. J Pediatr Orthop [Internet]. 2006;26(3):291–4. Available from: http://www.ncbi.nlm.nih.gov/pubmed/16670537
17. Gao J, Williams JL, Roan E. On the State of Stress in the Growth Plate under Physiologic Compressive Loading. 2014;2014(January):13–21.
18. Piszczatowski S. Geometrical aspects of growth plate modelling using Carter's and Stokes's approaches. Acta Bioeng Biomech / Wrocław Univ Technol [Internet]. 2012;14(1):93–106. Available from: http://www.ncbi.nlm.nih.gov/pubmed/22741593
19. Richmond BG, Wright BW, Grosse I, Dechow PC, Ross CF, Spencer M a, et al. Finite element analysis in functional morphology. Anat Rec A Discov Mol Cell Evol Biol [Internet]. 2005 Apr [cited 2012 Nov 13];283(2):259–74. Available from: http://www.ncbi.nlm.nih.gov/pubmed/15747355
20. Berthaume MA, Dumont ER, Godfrey LR, Grosse IR. How does tooth cusp radius of curvature affect brittle food item processing ? 2013;20–4.
21. Ledogar JA, Benazzi S, Smith AL, Weber GW, Carlson KB, Dechow PC, et al. The Biomechanics of Bony Facial " Buttresses " in South African Australopiths : An Experimental Study Using Finite Element Analysis. 2017;195(August 2016):171–95.
22. Barani A, Keown AJ, Bush MB, Lee JJ, Chai H, Lawn BR. Acta Biomaterialia Mechanics of longitudinal cracks in tooth enamel. Acta Biomater [Internet]. 2011;7(5):2285–92. Available from: http://dx.doi.org/10.1016/j.actbio.2011.01.038
23. Dumont ER, Samadevam K, Grosse I, Warsi OM, Baird B, Davalos LM. SELECTION FOR MECHANICAL ADVANTAGE UNDERLIES MULTIPLE CRANIAL OPTIMA IN NEW WORLD LEAF-NOSED BATS. 2014;1436–49.
24. Stayton CT. APPLICATION OF THIN-PLATE SPLINE TRANSFORMATIONS TO FINITE ELEMENT MODELS , OR , HOW TO TURN A BOG TURTLE INTO A SPOTTED TURTLE TO ANALYZE BOTH. 2009;1348–55.
25. Polly PD, Stayton CT, Dumont ER, Pierce SE, Rayfield EJ, Angielczyk KD. Combining geometric morphometrics and finite element analysis with evolutionary modeling: towards a synthesis. J Vertebr Paleontol. 2016;4634(March):0–23.
26. Sockol MD, Raichlen D a, Pontzer H. Chimpanzee locomotor energetics and the origin of human bipedalism. Proc Natl Acad Sci U S A [Internet]. 2007 Jul 24;104(30):12265–9. Available from: http://www.pubmedcentral.nih.gov/articlerender.fcgi?artid=1941460&tool=pmcentrez&rendertype=abstract
27. Doran D. The ontogeny of chimpanzee and pygmy chimpanzee locomotor behavior: a case study of paedomorphism and its behavioral correlates. J Hum Evol [Internet]. 1992 [cited 2013 Jan 5];(23):139–57. Available from: http://www.sciencedirect.com/science/article/pii/004724849290104H
28. Isler K. 3D-kinematics of vertical climbing in hominoids. Am J Phys Anthropol [Internet]. 2005 Jan [cited 2012 Nov 6];126(1):66–81. Available from: http://www.ncbi.nlm.nih.gov/pubmed/15386239
29. Yamazaki N, Ishida H. A biomechanical study of vertical climbing and bipedal walking in gibbons. J Hum Evol [Internet]. 1984 [cited 2013 Feb 13];563–71. Available from: http://www.sciencedirect.com/science/article/pii/S0047248484800287
30. Shea BT. Relative growth of the limbs and trunk in the African apes. Am J Phys Anthropol [Internet]. 1981 Oct;56(2):179–201. Available from:

http://www.ncbi.nlm.nih.gov/pubmed/7325219
31. Green DJ. Ontogeny of the hominoid scapula: The influence of locomotion on morphology. Am J Phys Anthropol [Internet]. 2013 Oct [cited 2014 Feb 19];152(2):239–60. Available from: http://www.ncbi.nlm.nih.gov/pubmed/24000155
32. Sissons HA, Kember NF. Longitudinal bone growth of the human femur. Postgrad Med J. 1977;53(August):433–6.
33. Piszczatowski S. Material aspects of growth plate modelling using Carter's and Stokes's approaches. Acta Bioeng Biomech / Wrocław Univ Technol [Internet]. 2011;13(3):3–14. Available from: http://www.ncbi.nlm.nih.gov/pubmed/22097913
34. Trepczynski A, Kutzner I, Kornaropoulos E, Taylor WR, Duda GN, Bergmann G, et al. Patellofemoral joint contact forces during activities with high knee flexion. J Orthop Res. 2012;(March):408–15.
35. Goodfellow J, Hungerford DS, Zindel M. Patello-Femoral Joint Mechanics and Pathology. J Bone Jt Surg. 1976;58-B(3):287–90.
36. Lenhart RL, Brandon SCE, Smith CR, Novacheck TF, Schwartz MH, Thelen DG. Influence of patellar position on the knee extensor mechanism in normal and crouched walking. J Biomech [Internet]. 2017;51:1–7. Available from: http://dx.doi.org/10.1016/j.jbiomech.2016.11.052
37. Dumont ER, Grosse IR, Slater GJ. Requirements for comparing the performance of finite element models of biological structures. J Theor Biol. 2009;256(1):96–103.
38. Shan S, Kovalsky SZ, Winchester JM, Boyer DM, Daubechies I. ariaDNE: A robustly implemented algorithm for Dirichlet energy of the normal. Methods Ecol Evol. 2019;10(4):541–52.
39. Winchester JM. MorphoTester: An Open Source Application for Morphological Topographic Analysis. PLoS One [Internet]. 2016;11(2):e0147649. Available from: http://dx.plos.org/10.1371/journal.pone.0147649
40. R Core Team. R: A Language and Environment for Statistical Computing [Internet]. Vienna, Austria: R Foundation for Statistical Computing; 2018. Available from: https://www.r-project.org
41. McElreath R. Statistical Rethinking. Second. 2017.
42. Raichlen DA, Gordon AD, Foster AD, Webber JT, Sukhdeo SM, Scott RS, et al. An ontogenetic framework linking locomotion and trabecular bone architecture with applications for reconstructing hominin life history. J Hum Evol [Internet]. 2015;81:1–12. Available from: http://dx.doi.org/10.1016/j.jhevol.2015.01.003
43. Cowgill LW, Warrener AG, Pontzer H, Ocobock C. Waddling and toddling: the biomechanical effects of an immature gait. Am J Phys Anthropol [Internet]. 2010 Sep [cited 2012 Nov 19];143(1):52–61. Available from: http://www.ncbi.nlm.nih.gov/pubmed/20310059
44. Beaupre GS, Stevens SS, Carter DR. Department of Mechanobiology in the development , maintenance , and degeneration of articular cartilage. 2000;65(1).
45. Shefelbine SJ, Tardieu C, Carter DR. Development of the femoral bicondylar angle in hominid bipedalism. Bone [Internet]. 2002 May;30(5):765–70. Available from: http://www.ncbi.nlm.nih.gov/pubmed/11996917
46. Villemure I, Stokes I a F. Growth plate mechanics and mechanobiology. A survey of present understanding. J Biomech [Internet]. 2009 Aug 25 [cited 2012 Dec 14];42(12):1793–803. Available from:

http://www.pubmedcentral.nih.gov/articlerender.fcgi?artid=2739053&tool=pmcentrez&rendertype=abstract
47. Alemseged Z, Spoor F, Kimbel WH, Bobe R, Geraads D, Reed D, et al. A juvenile early hominin skeleton from Dikika, Ethiopia. Nature [Internet]. 2006 Sep 21 [cited 2012 Nov 6];443(7109):296–301. Available from: http://www.ncbi.nlm.nih.gov/pubmed/16988704
48. Latimer BM. Locomotor adaptations in Australopithecus afarensis - the issue of arboreality. In: Origine(s) de la Bipedie chez les Hominides. 1991.
49. Ward C V. Postcranial and Locomotor Adaptation of Hominoids. In: Handbook of Paleoanthropology. 2007.
50. Lovejoy CO, Heiple KG, Burstein AH. The gait of Australopithecus. Am J Phys Anthropol [Internet]. 1973 May;38(3):757–79. Available from: http://www.ncbi.nlm.nih.gov/pubmed/4735528
51. Stern JT, Susman RL. The locomotor anatomy of Australopithecus afarensis. Am J Phys Anthropol [Internet]. 1983 Mar;60(3):279–317. Available from: http://www.ncbi.nlm.nih.gov/pubmed/6405621
52. Ruff CB, Burgess ML, Bromage TG, Mudakikwa A, McFarlin SC. Ontogenetic changes in limb bone structural proportions in mountain gorillas (Gorilla beringei beringei). J Hum Evol [Internet]. 2013 Dec [cited 2014 Feb 19];65(6):693–703. Available from: http://www.ncbi.nlm.nih.gov/pubmed/24129040
53. Green DJ, Alemseged Z. Australopithecus afarensis scapular ontogeny, function, and the role of climbing in human evolution. Science (80-) [Internet]. 2012 Oct 26 [cited 2013 Jan 6];338:514–7. Available from: http://www.sciencemag.org/cgi/doi/10.1126/science.1227123

Tables and Figures

Table 1: Specimens and associated metrics and data. All stresses are in MPa. Institution codes: DUND (University of Dundee), UKEN (University of Kentucky), MPI (Max Planck Institute), RMCA (Musée Royal de l'Afrique Centrale).

Specimen ID	Genus	Sex	ariaDNE	Surface area (mm^3)	Model	Max von Mises stress	Mean von Mises stress	Scaled Max von Mises stress	Scaled Mean von Mises stress
DUND SC-010	Homo	U	0.0397	907.02	walk	0.0708	0.0340	0.0664	0.0318
					climb	0.1974	0.1209	0.1850	0.1133
DUND SC-026	Homo	F	0.03007	967.74	walk	0.0636	0.0318	0.0636	0.0318
					climb	0.1766	0.1165	0.1766	0.1165
UKEN OH2 225	Homo	U	0.04173	640.59	walk	0.0839	0.0411	0.0555	0.0272
					climb	0.2622	0.1616	0.1736	0.1070
UKEN OH2 035	Homo	U	0.03896	506.78	walk	0.1333	0.0586	0.0698	0.0307
					climb	0.3357	0.2298	0.1758	0.1203
UKEN OH2 505	Homo	U	0.03252	628.99	walk	0.0976	0.0466	0.0635	0.0303
					climb	0.3180	0.1808	0.2067	0.1175
UKEN OH2 622	Homo	U	0.03376	638.25	walk	0.0897	0.0408	0.0592	0.0269
					climb	0.2289	0.1692	0.1510	0.1116
MPI 11777	Pan	M	0.04994	359.63	walk	0.2059	0.0678	0.0765	0.0252
					climb	0.3441	0.1998	0.1279	0.0743
MPI 13432	Pan	M	0.05673	339.32	walk	0.2152	0.0720	0.0754	0.0253
					climb	0.3440	0.2086	0.1206	0.0731
RMCA 302	Pan	F	0.05168	400.32	walk	0.2038	0.0847	0.0843	0.0350
					climb	0.3452	0.1735	0.1428	0.0718
RMCA 11293	Pan	M	0.04981	250.31	walk	0.2818	0.1009	0.0729	0.0261
					climb	0.4151	0.2294	0.1074	0.0593
RMCA 22336	Pan	U	0.06848	292.52	walk	0.2105	0.0654	0.0636	0.0198
					climb	0.3256	0.1654	0.0984	0.0500

Table 2: Statistical results for maximum von Mises stress at the growth plate.

	Mean	Std. dev.	2.5%	97.5%
Homo-Climb	0.178	0.006	0.166	0.190
Homo-Walk	0.063	0.006	0.051	0.075
Pan-Climb	0.119	0.006	0.106	0.132
Pan-Walk	0.074	0.007	0.061	0.087
Ratio Homo-Climb/ Homo-Walk	2.851	0.298	2.341	3.507
Ratio Pan-Climb/Pan-Walk	1.616	0.174	1.312	1.995
Ratio Homo-Walk/Pan-Walk	0.853	0.113	0.652	1.097
Ratio Homo-Climb/Pan - Climb	1.496	0.096	1.318	1.698

Table 3: Statistical results for mean von Mises stress at the growth plate.

	Mean	Std. dev.	2.5%	97.5%
Homo-Climb	0.114	0.003	0.109	0.120
Homo-Walk	0.030	0.003	0.024	0.035
Pan-Climb	0.066	0.003	0.059	0.072
Pan-Walk	0.026	0.003	0.020	0.032
Ratio Homo-Climb/ Homo-Walk	3.867	0.386	3.208	4.722
Ratio Pan-Climb/Pan-Walk	2.536	0.337	1.980	3.309
Ratio Homo-Walk/Pan-Walk	1.152	0.180	0.844	1.548
Ratio Homo-Climb/Pan - Climb	1.745	0.094	1.570	1.945

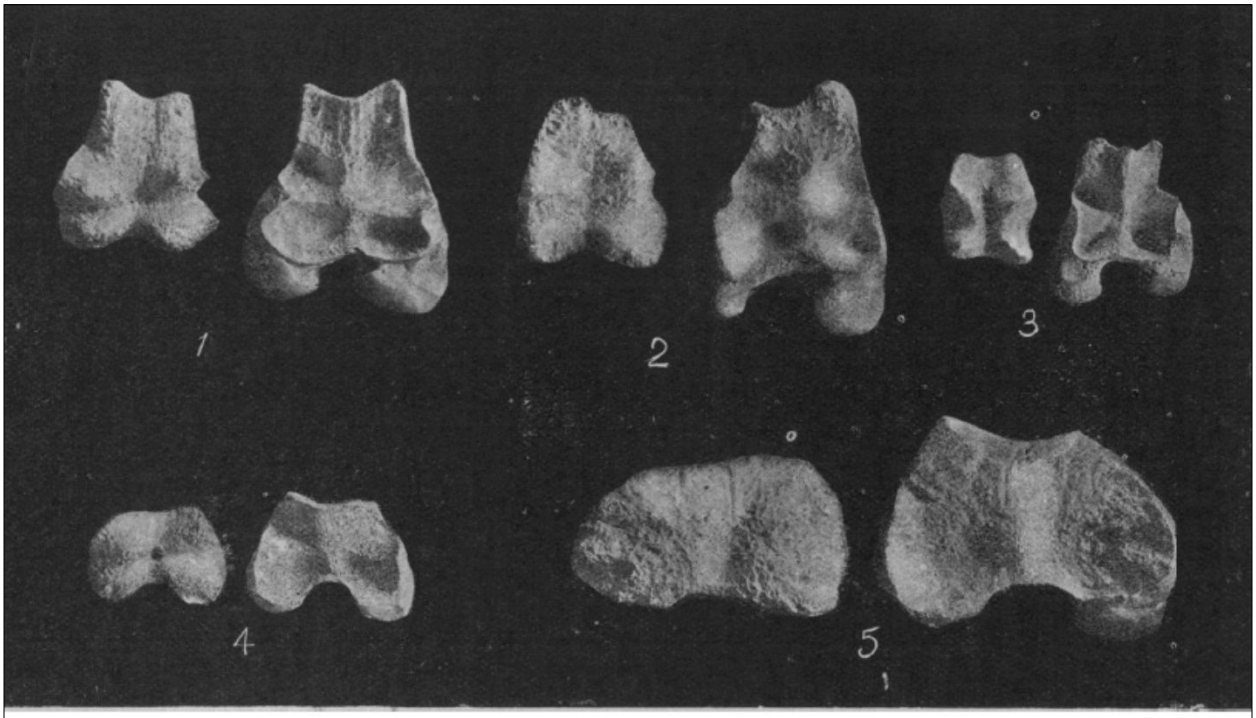

FIG. 1.—Photographs of the lower end of the femoral diaphysis and upper surface of the inferior femoral epiphysis. 1, mouflon ; 2, red deer ; 3, wolf ; 4, baboon ; 5, man.

Figure 1: Thomson (5) was the first to write of the divergent morphologies found in the distal metaphyseal surfaces of the femur of mammals. Reproduced with permission.

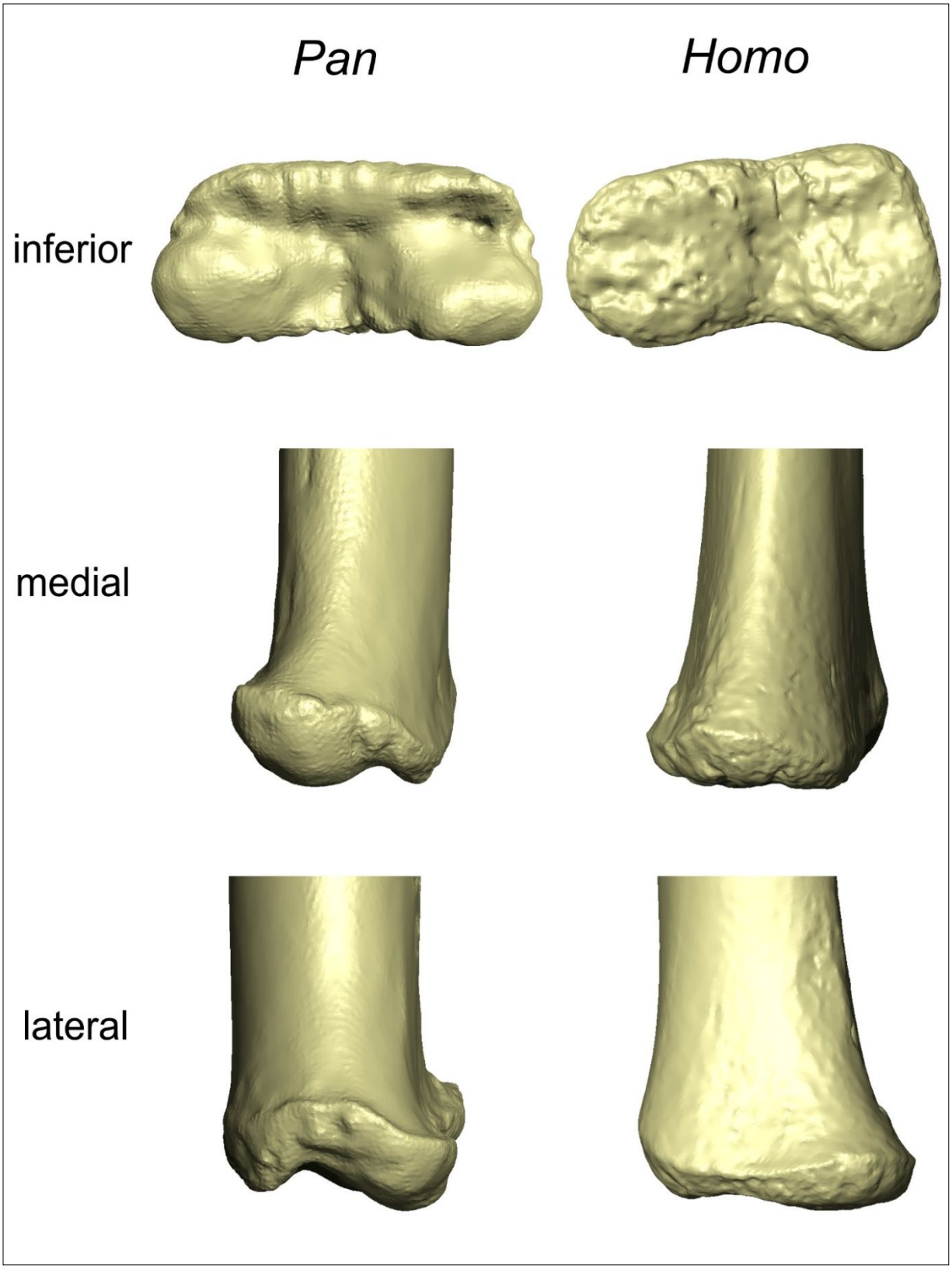

Figure 2: 3D models created from surface scans of the distal femora of *Pan* and *Homo* juveniles. These individuals are representative of their respective genera in our sample.

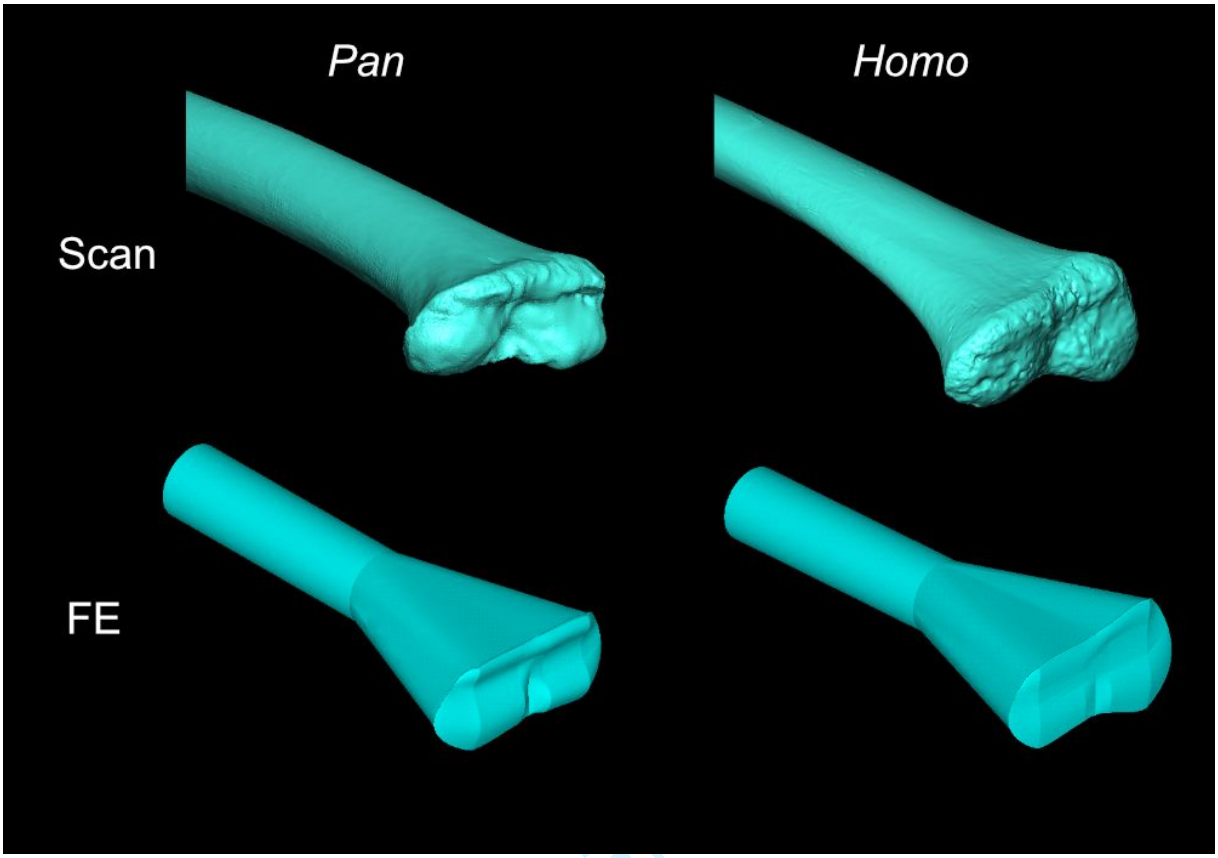

Figure 3: A comparison of the surface scan derived (top) and parametric finite element model (bottom) of representative *Pan* and *Homo* specimens in our sample. While the epiphysis and growth plate were modeled, those have been stripped away to show the morphology of the distal metaphyseal surface.

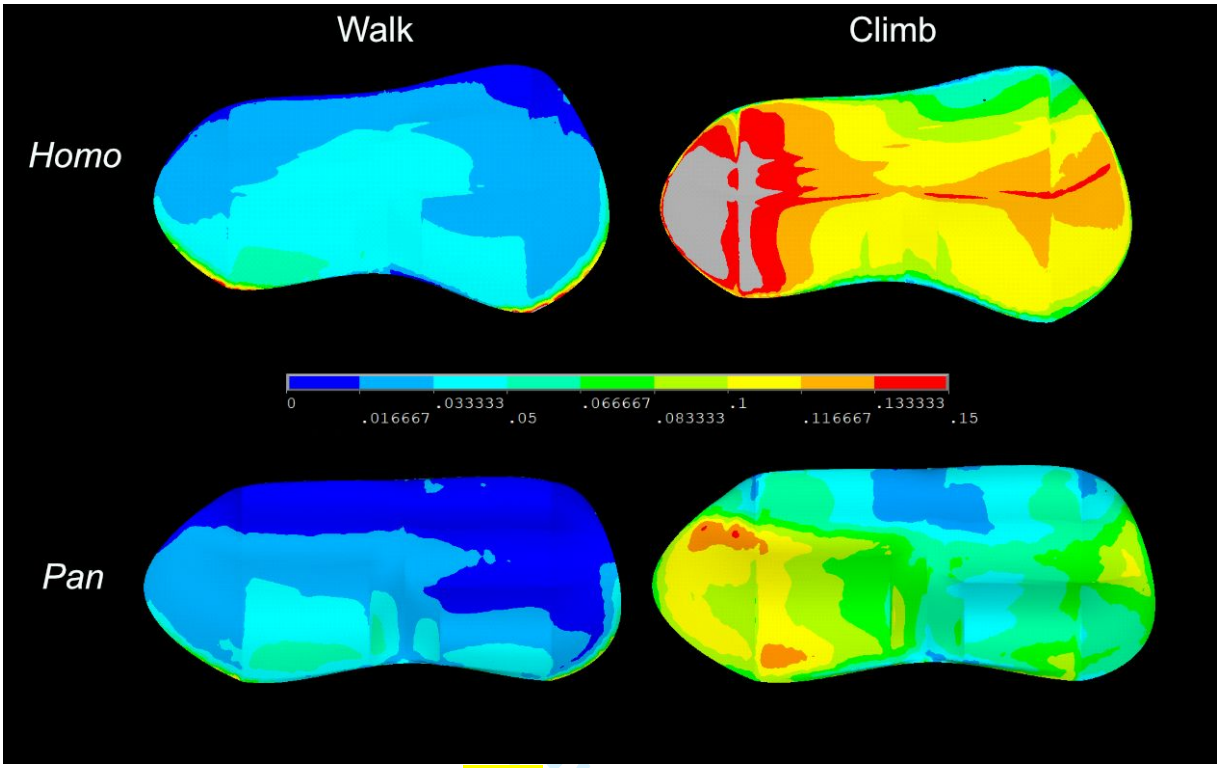

Figure 4: Heat maps comparing the scaled von Mises stress (MPa) distribution across the growth plates of *Homo* and *Pan* individuals under simulated walking and climbing loads. While there is little inter-taxon difference in the stresses during walking, during climbing the *Homo* growth plate is subjected to markedly higher stresses than that of *Pan*. Stresses have been scaled following the protocol in Dumont et al. (37).

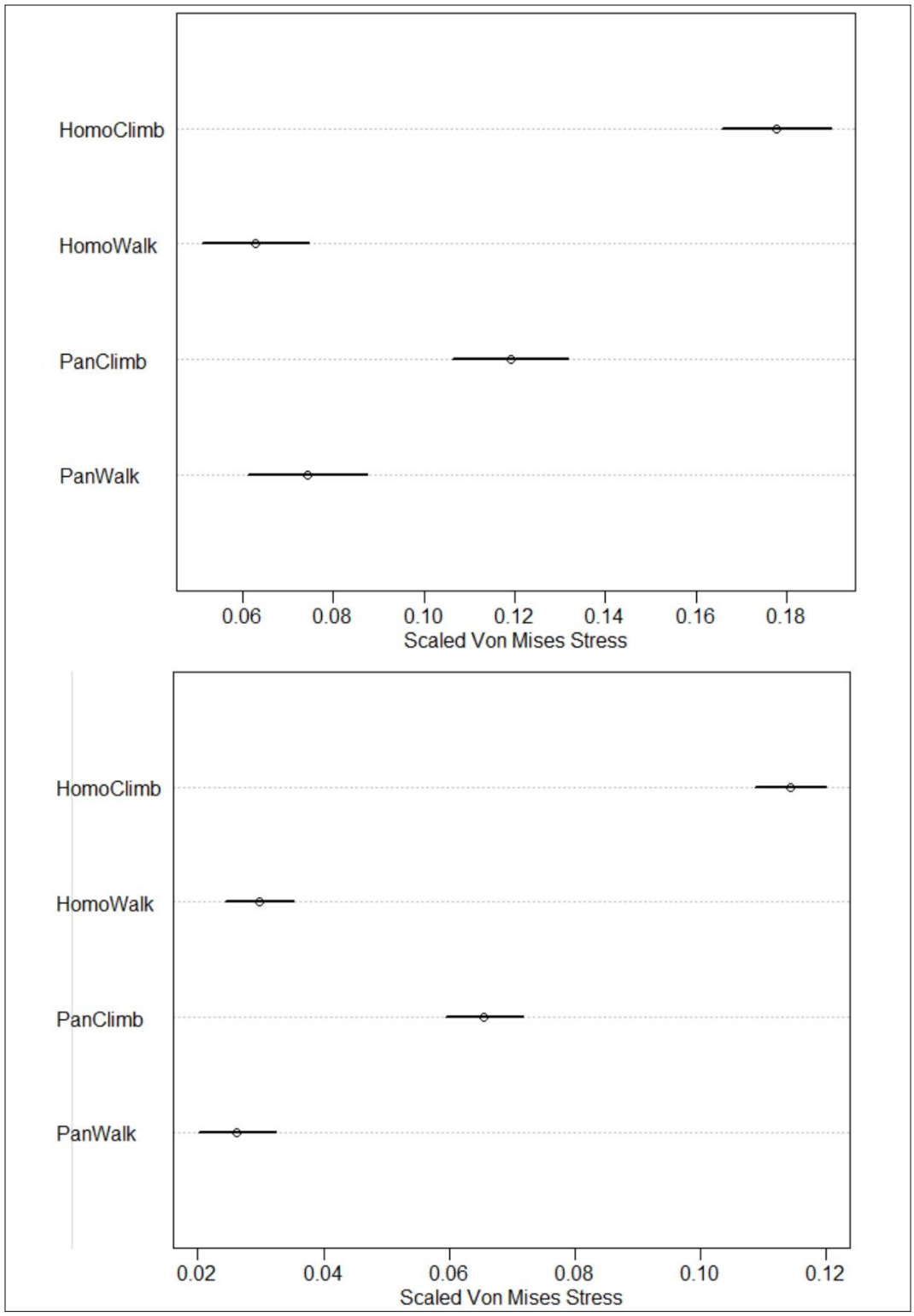

Figure 5: Maximum (top) and Mean (bottom) von Mises stress (MPa) at the growth plate across each taxon and loading condition. The point shows the maximum *a posteriori* estimate, while the bar shows the 95% credibility interval of that estimate. Our results show (1) that walking is significantly less stressful than climbing, and (2) that the *Pan* morphology acts to reduce both maximum and mean von Mises stresses at the growth plate during climbing.

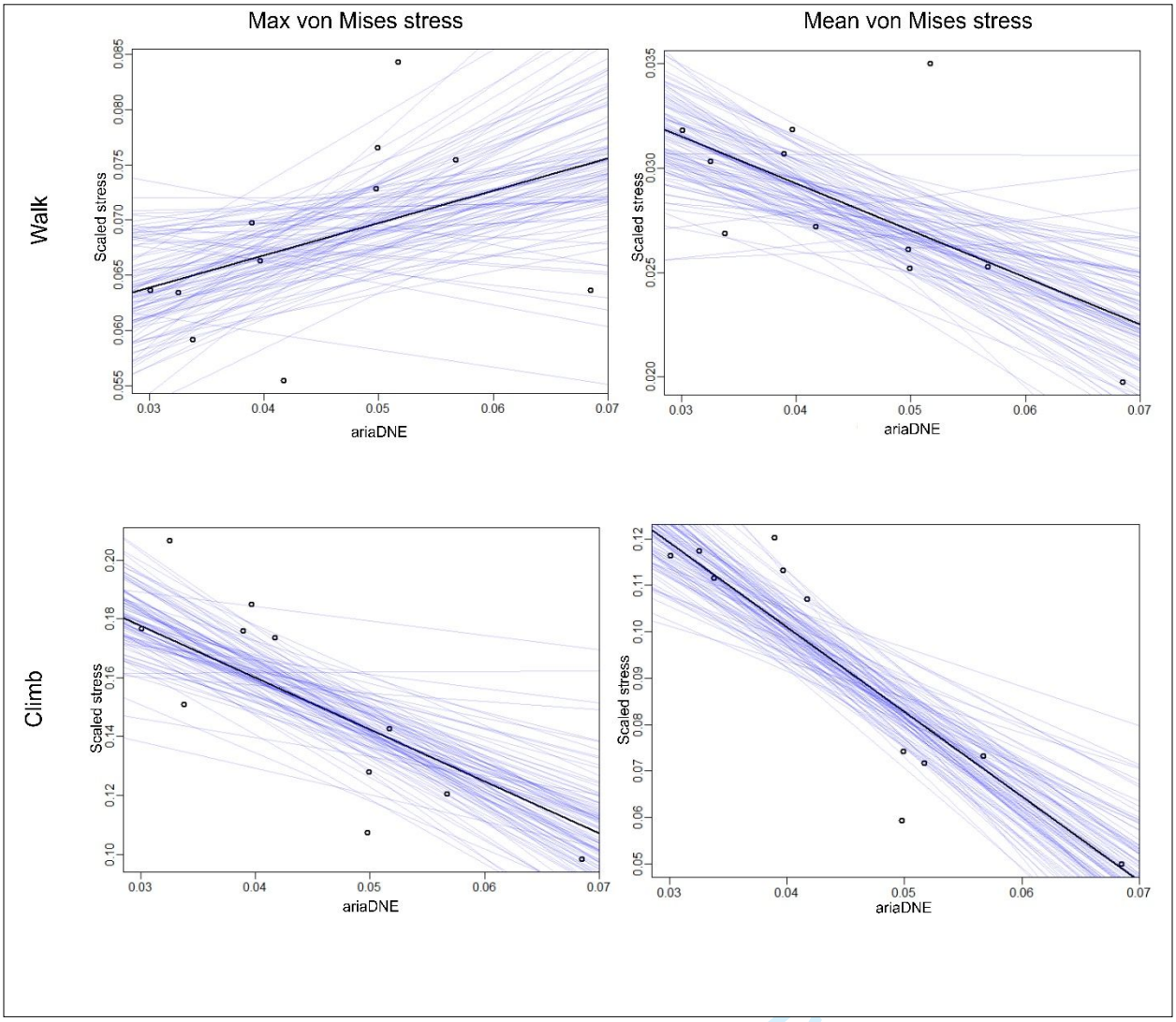

Figure 6: The relationship between complexity as quantified by ariaDNE and maximum (left) and mean (right) von Mises stress (MPa) at the growth plate during simulated walking (top) and climbing (bottom) loads. The black line represents the maximum *a posteriori* relationship, while each blue line is 1 of 95 sampled from the posterior distribution.

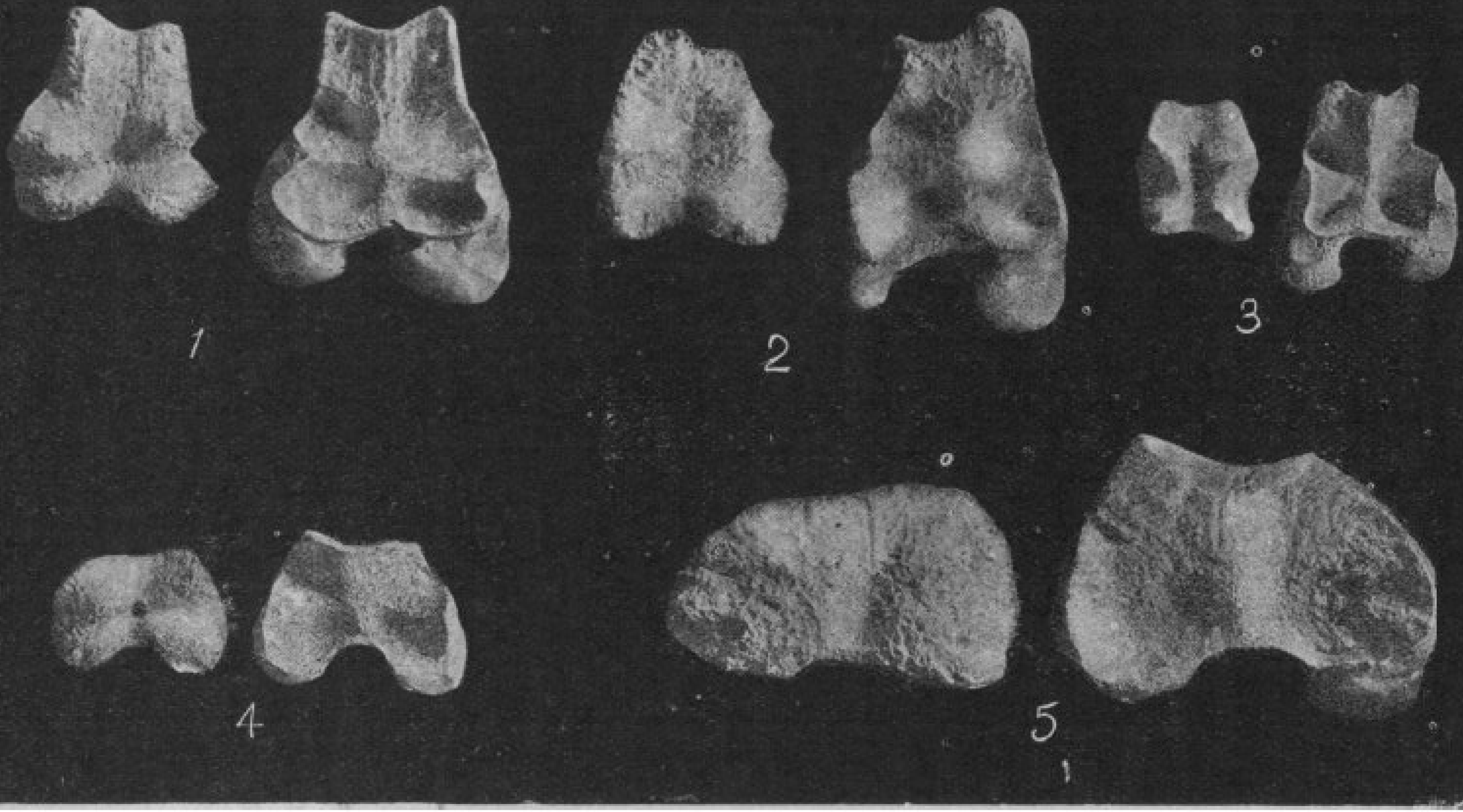

FIG. 1.—Photographs of the lower end of the femoral diaphysis and upper surface of the inferior femoral epiphysis. 1, mouflon ; 2, red deer ; 3, wolf ; 4, baboon ; 5, man.

Pan *Homo*

inferior

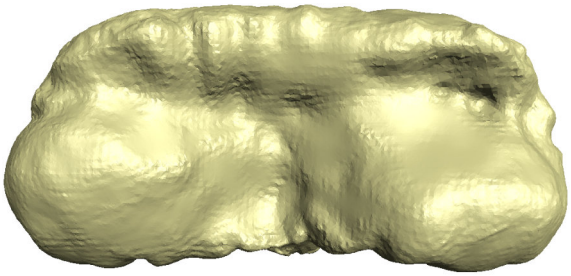

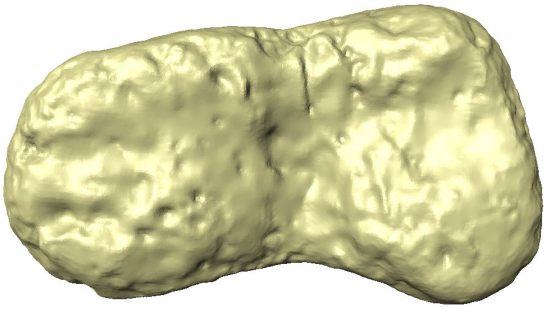

medial

lateral

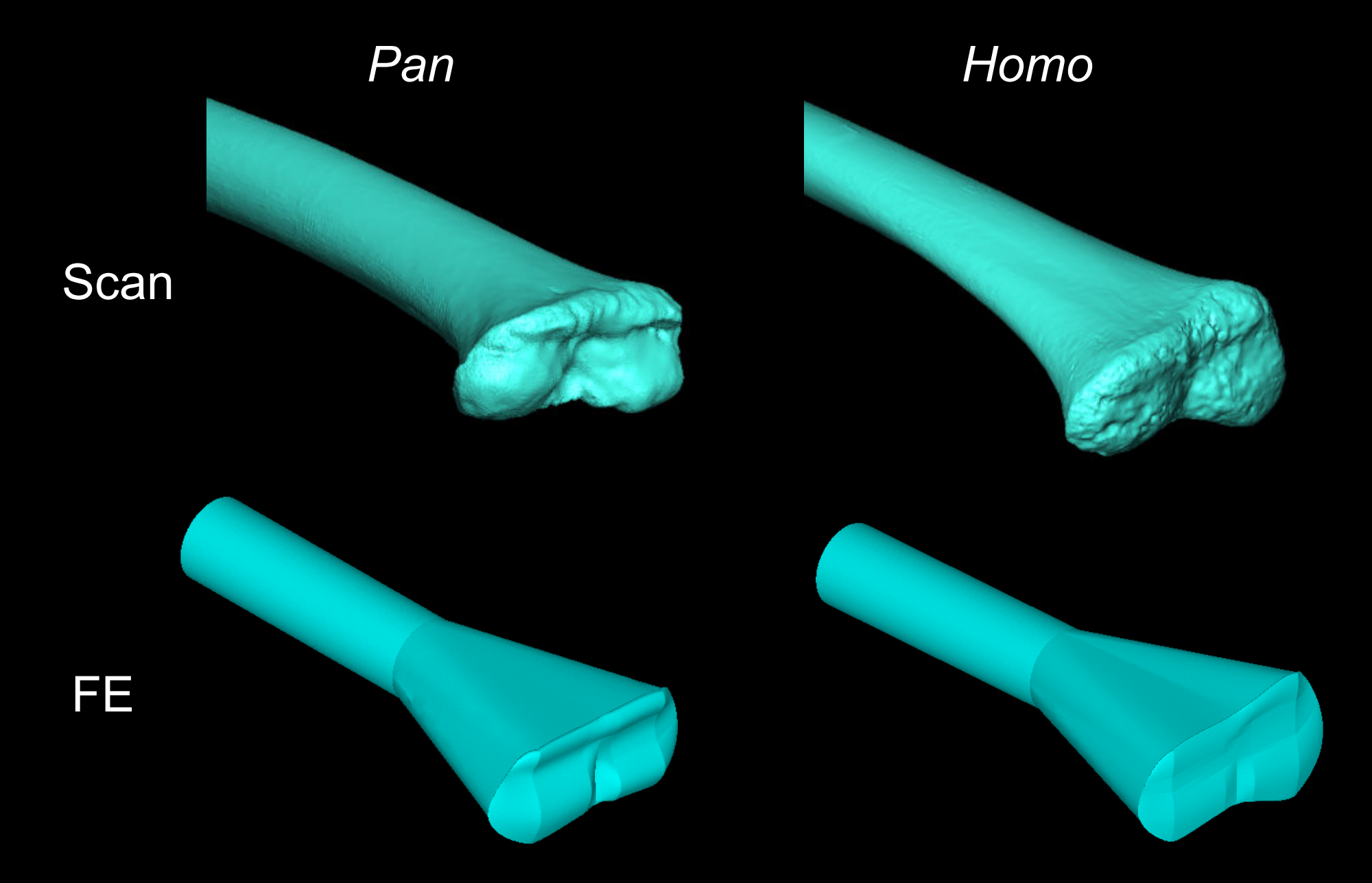
Pan
Homo
Scan
FE

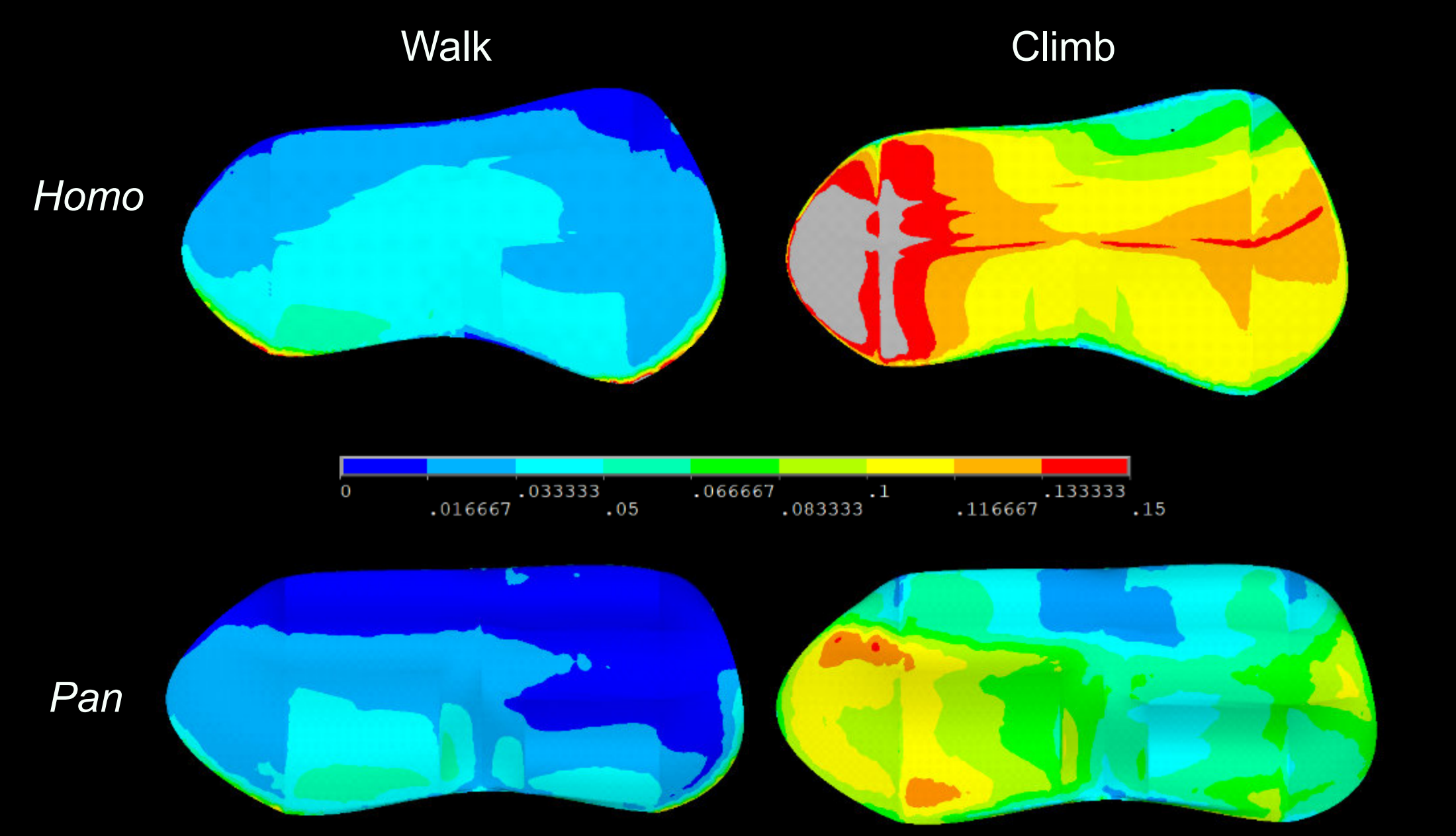
Walk
Climb
Homo
Pan
0
.016667
.033333
.05
.066667
.083333
.1
.116667
.133333
.15

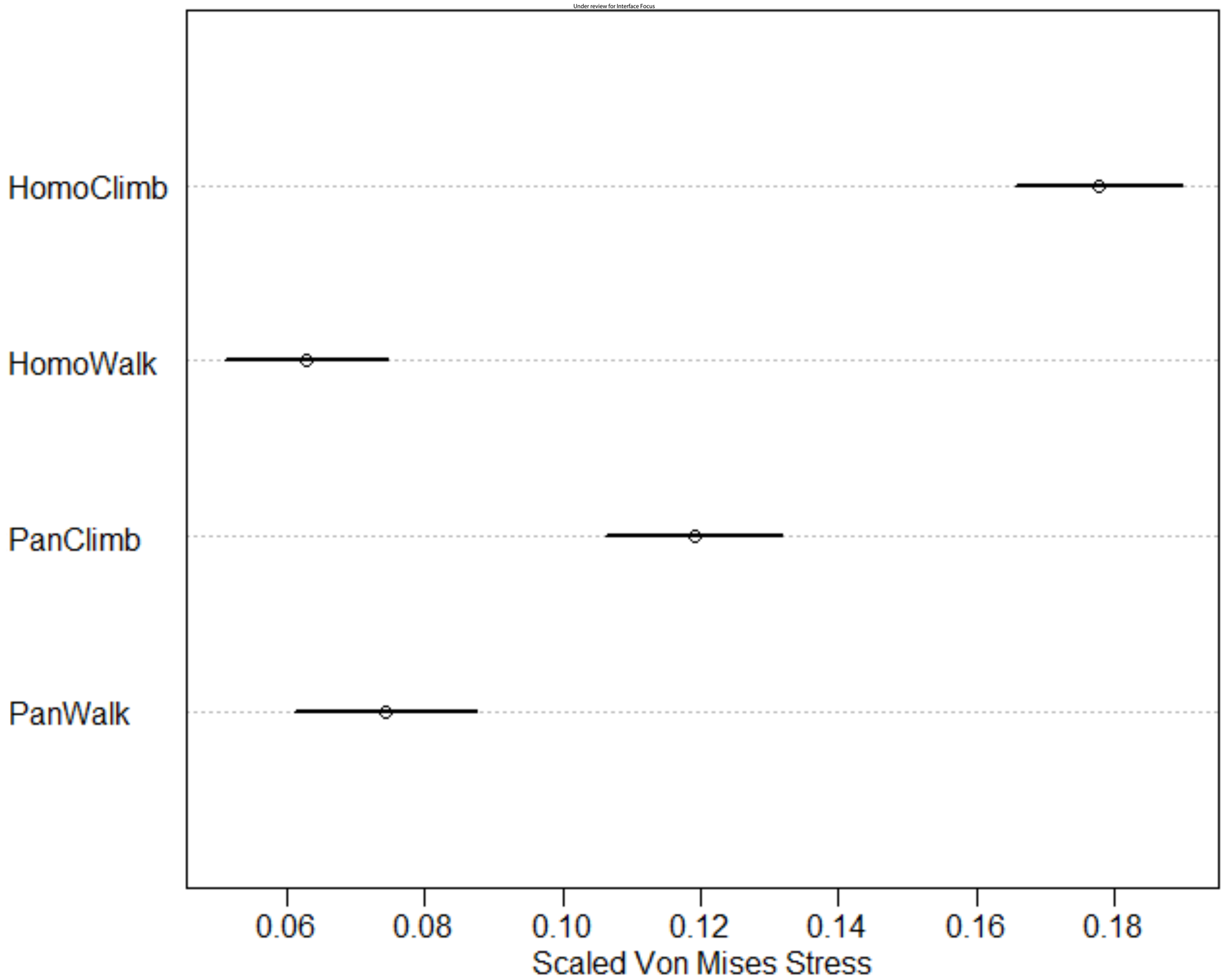
HomoClimb
HomoWalk
PanClimb
PanWalk
0.06
0.08
0.10
0.12
0.14
0.16
0.18
Scaled Von Mises Stress

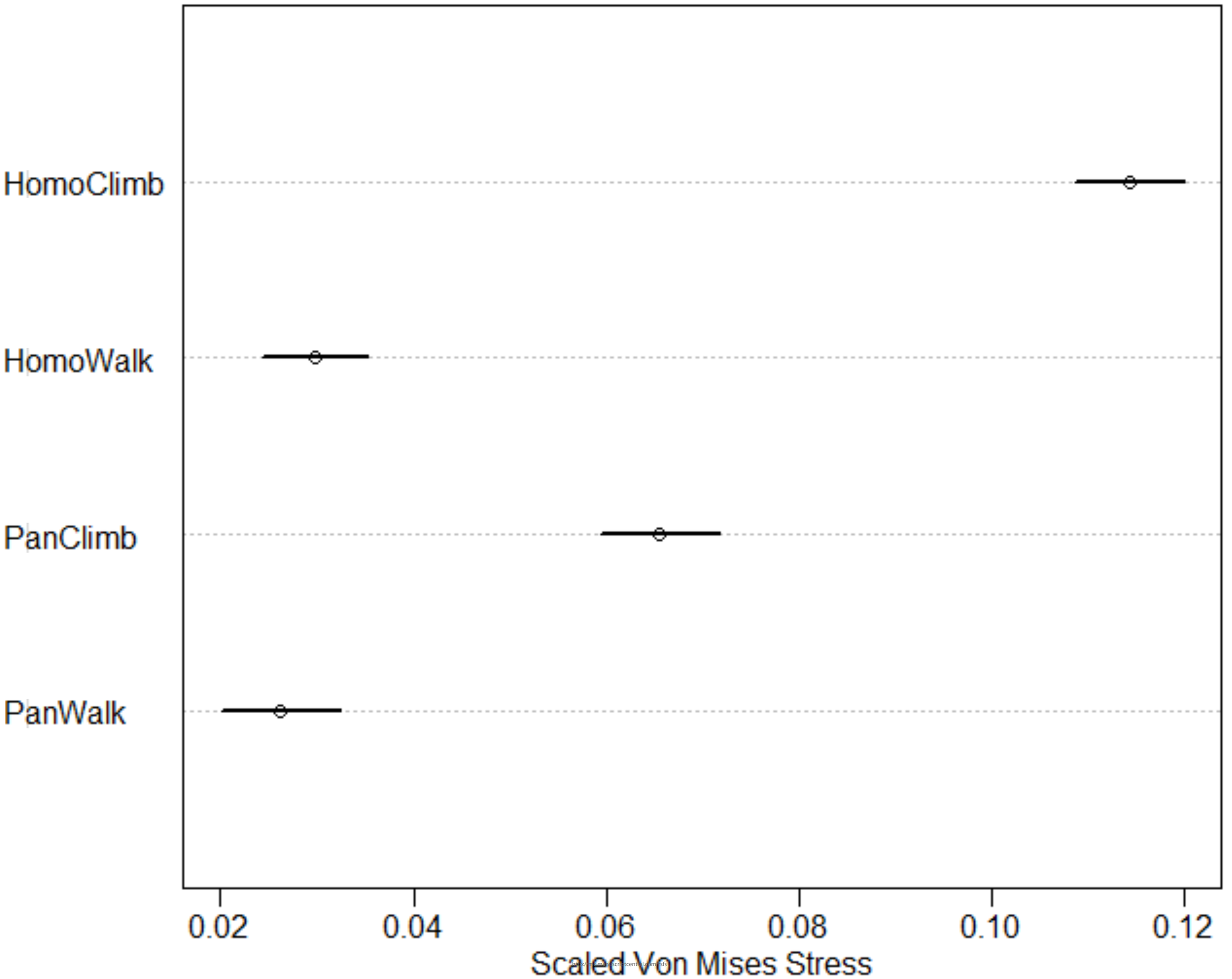
HomoClimb
HomoWalk
PanClimb
PanWalk
0.02
0.04
0.06
0.08
0.10
0.12
Scaled Von Mises Stress

Walk

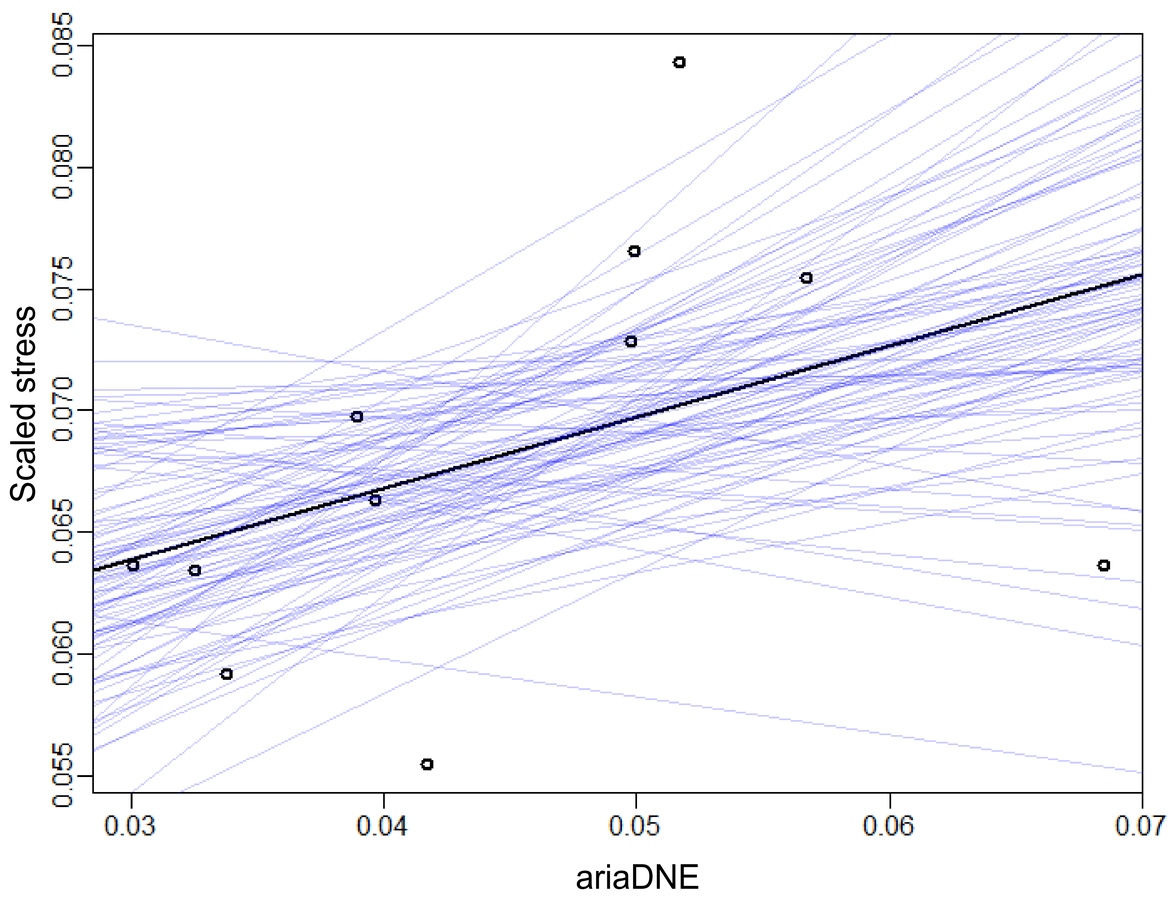
Max von Mises stress
Scaled stress
0.055
0.060
0.065
0.070
0.075
0.080
0.085
0.03
0.04
0.05
0.06
0.07
ariaDNE

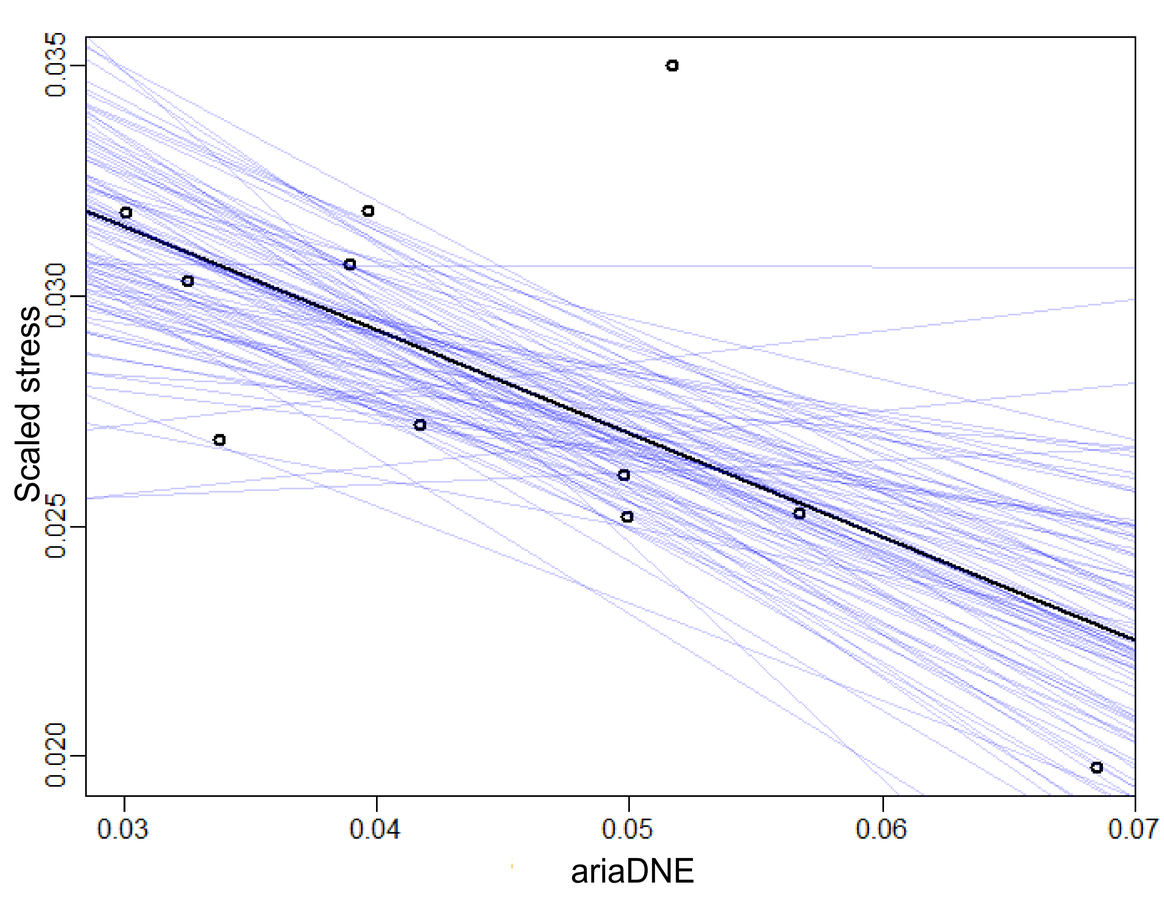
Mean von Mises stress
Scaled stress
0.020
0.025
0.030
0.035
0.03
0.04
0.05
0.06
0.07
ariaDNE

Climb

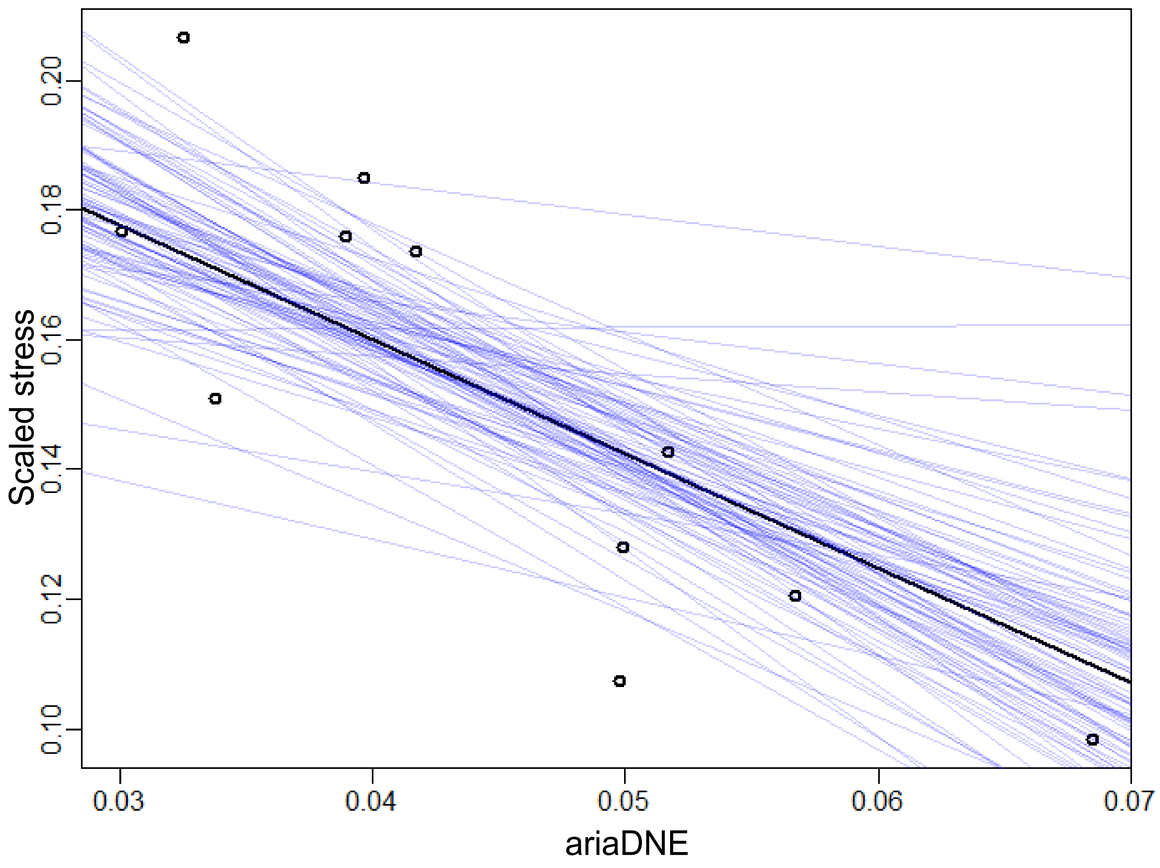
Scaled stress
0.10
0.12
0.14
0.16
0.18
0.20
0.03
0.04
0.05
0.06
0.07
ariaDNE

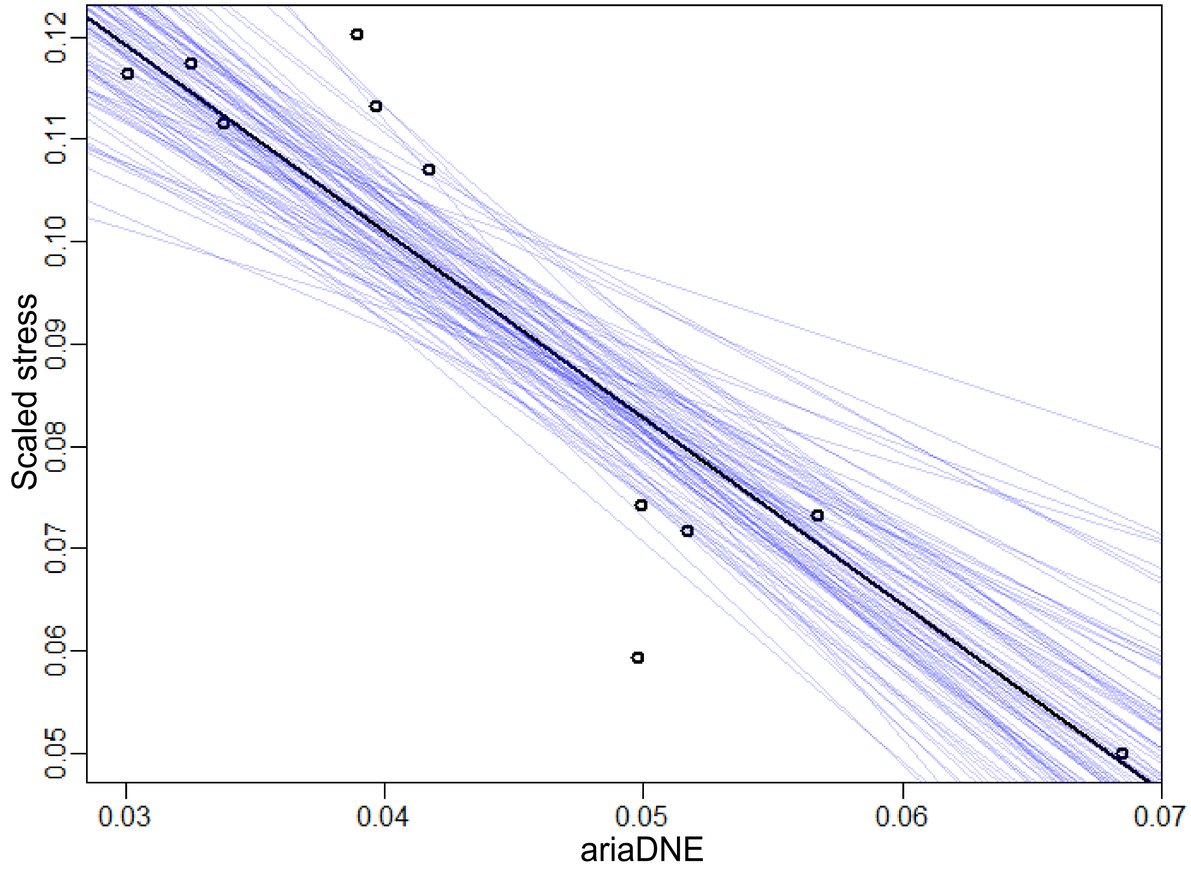
Scaled stress
0.05
0.06
0.07
0.08
0.09
0.10
0.11
0.12
0.03
0.04
0.05
0.06
0.07
ariaDNE